(Micro-)plastics in saturated and unsaturated groundwater bodies: first evidence of presence in groundwater fauna and habitats

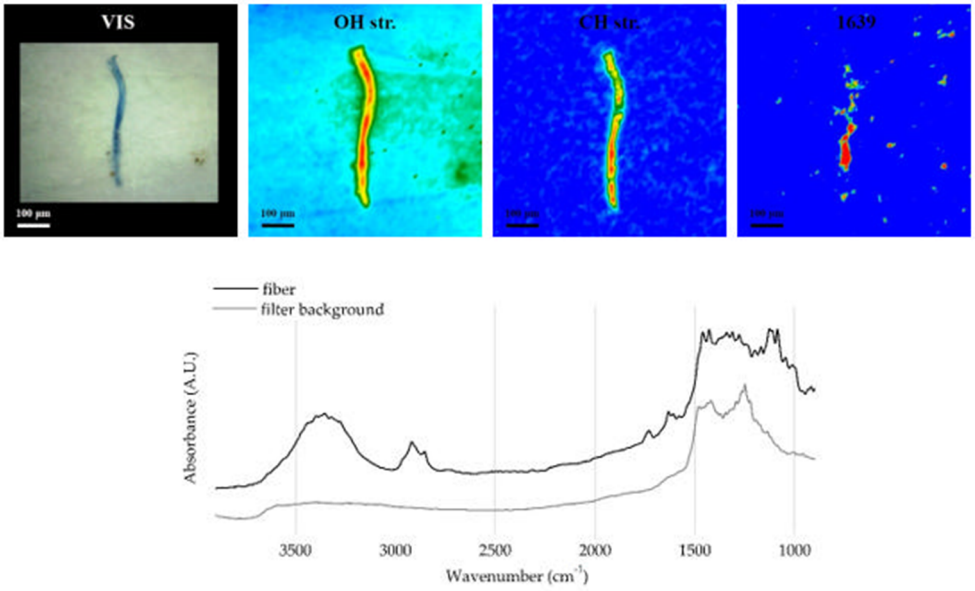

Figure S1. (From the left) Visible light and 2D FTIR Imaging maps of a fiber identified as textile/artificial cellulose owing to absorption 3500-3000 cm^{-1} (OH stretching), 3000-2800 cm^{-1} (CH stretching), 1727 cm^{-1} (C=O stretching), 1639 cm^{-1} (adsorbed water), 1459 and 1434 cm^{-1} (CH bending), and 1091 cm^{-1} (C-OH stretching) [91]. (Bottom) FTIR Reflectance spectra of the polymer fiber and of the filter background, relating to a single pixel (5.5 × 5.5 μm^2) of the 2D Imaging map.

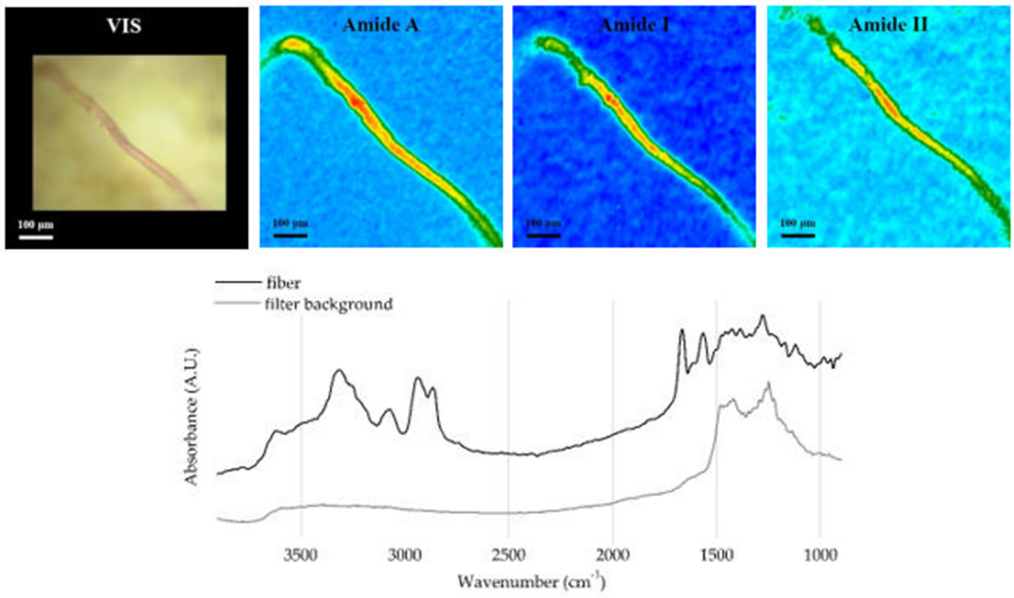

Figure S2. (From the left) Visible light and 2D FTIR Imaging maps of a fiber identified as polyamide (PA) owing to absorption 3306 cm^{-1} (Amide A), 3063 cm^{-1} (asymmetric CH stretching), 3000-2800 cm^{-1} (CH stretching), 1671 cm^{-1} (Amide I), 1565 cm^{-1} (Amide II), 1284 cm^{-1} (NH bending, C-N stretching), and 1172 cm^{-1} (CH_2 bending) [91]. (Bottom) FTIR Reflectance spectra of the polymer fiber and of the filter background, relating to a single pixel (5.5 × 5.5 μm^2) of the 2D Imaging map.

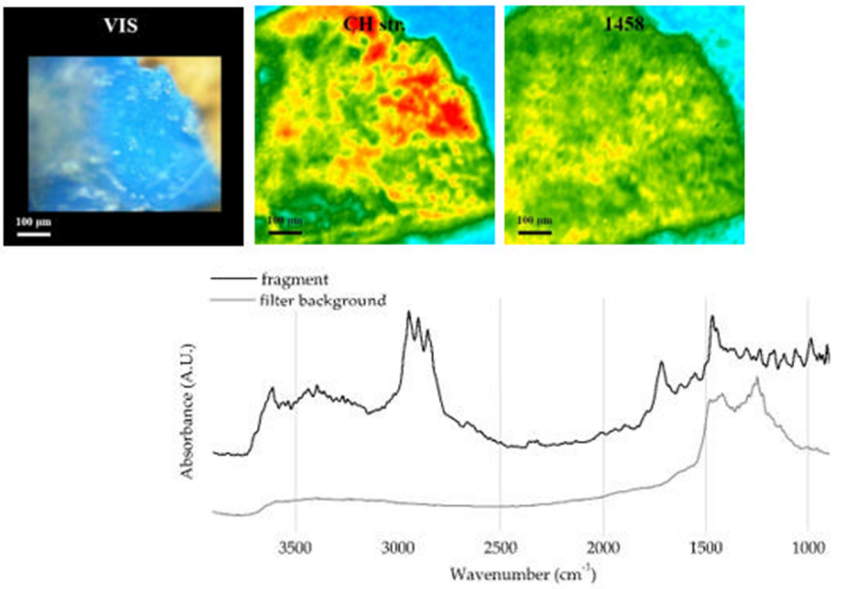

Figure S3. (From the left) Visible light and 2D FTIR Imaging maps of a fragment identified as polyethylene (PE) owing to absorption 2950-2800 cm^{-1} (CH stretching), 1715 cm^{-1} (C=O stretching, probably due to oxidation), 1458 cm^{-1} (CH_2 bending), and 1166 cm^{-1} (wagging deformation) [91,92]. (Bottom) FTIR Reflectance spectra of the polymer fragment and of the filter background, relating to a single pixel (5.5 × 5.5 μm^2) of the 2D Imaging map.

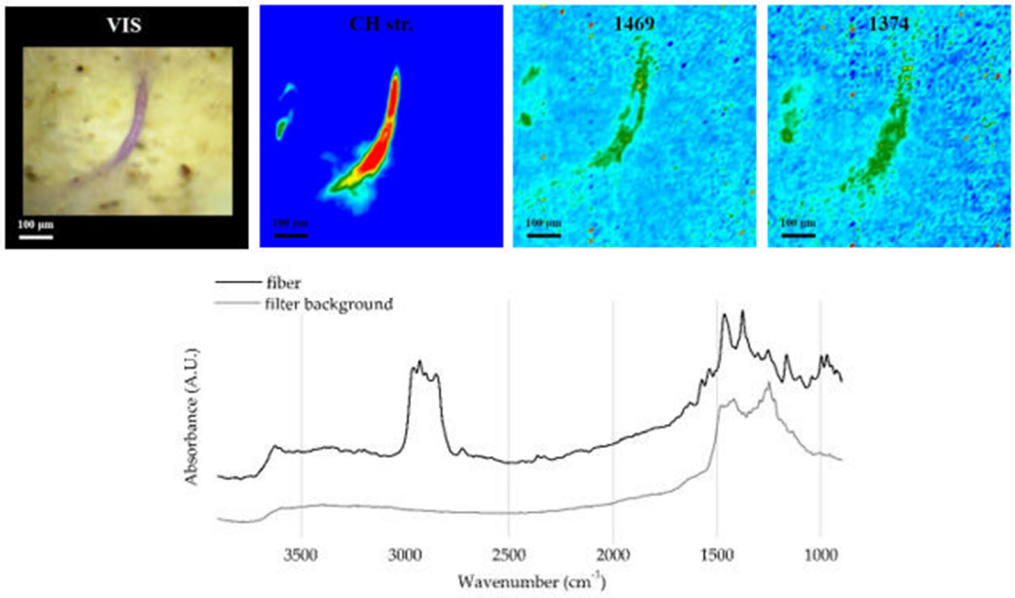

Figure S4. (From the left) Visible light and 2D FTIR Imaging maps of a fiber identified as polypropylene (PP) owing to absorption 3000-2800 cm^{-1} (CH stretching), 1715 cm^{-1} (C=O stretching, probably due to oxidation), 1469 cm^{-1} (CH_2 bending), 1374 cm^{-1} (CH_3 bending), 1253 cm^{-1} (CH_2 twist) and 1170 cm^{-1} (CH bending, CH_3 rocking, C-C stretching) [91,92]. (Bottom) FTIR Reflectance spectra of the polymer fiber and of the filter background, relating to a single pixel (5.5 × 5.5 μm^2) of the 2D Imaging map.

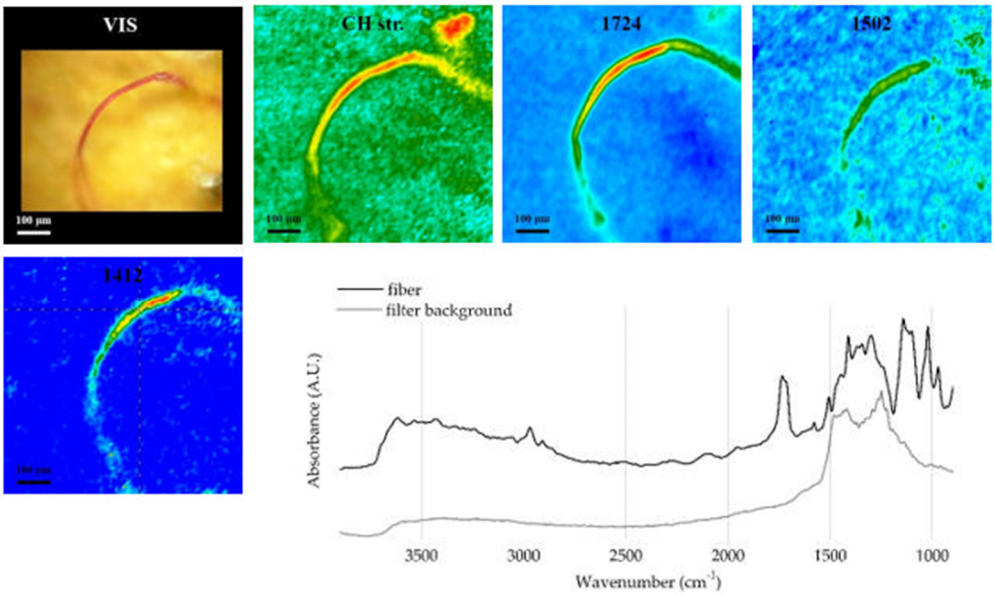

Figure S5. (From the left) Visible light and 2D FTIR Imaging maps of a fiber identified as polyethylene terephthalate (PET) owing to absorption 3000-2950 cm^{-1} (CH stretching), 1724 cm^{-1} (C=O stretching), 1571 and 1502 cm^{-1} (vibrations aromatic skeleton with stretching C=C), 1412 cm^{-1} (stretching of the C-O group deformation of the O-H group, and bending and wagging vibrational modes of the ethylene glycol segment), 1297 and 1141 cm^{-1} (terephthalate Group $OOCC_6H_4$-COO) [91]. (Bottom) FTIR Reflectance spectra of the polymer fiber and of the filter background, relating to a single pixel (5.5 × 5.5 μm^2) of the 2D Imaging map.

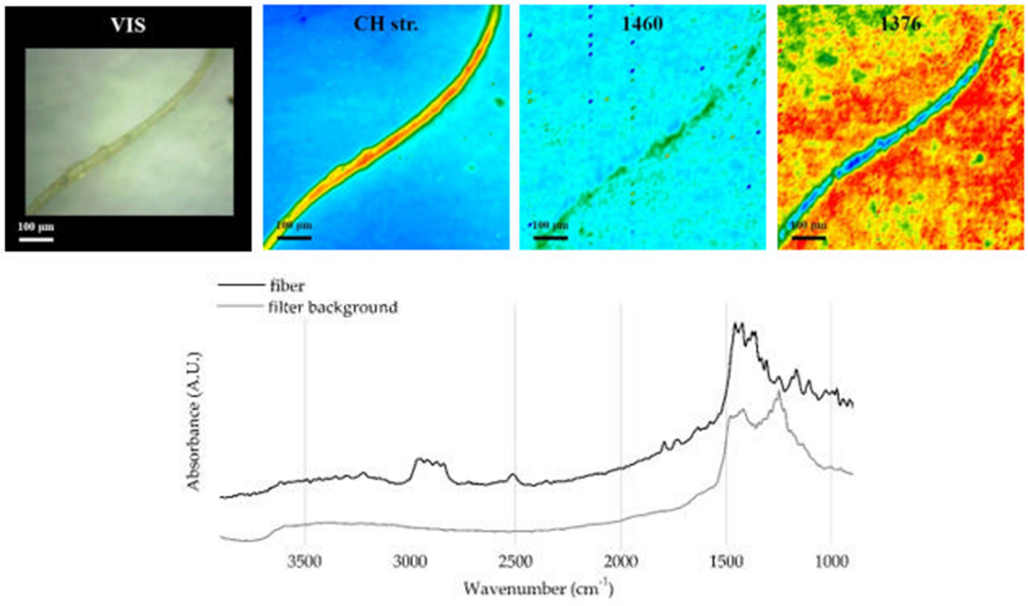

Figure S6. (From the left) Visible light and 2D FTIR Imaging maps of a fiber identified as polymeric blend of polypropylene and polyethylene (PE/PP) owing to absorption 3000-2800 cm^{-1} (CH stretching), 1791 cm^{-1} (C=O stretching probably due to oxidation), 1460 cm^{-1} (CH_2 bending), and 1376 cm^{-1} (CH_3 bending) [91]. (Bottom) FTIR Reflectance spectra of the polymer fiber and of the filter background, relating to a single pixel (5.5 × 5.5 μm^2) of the 2D Imaging map.

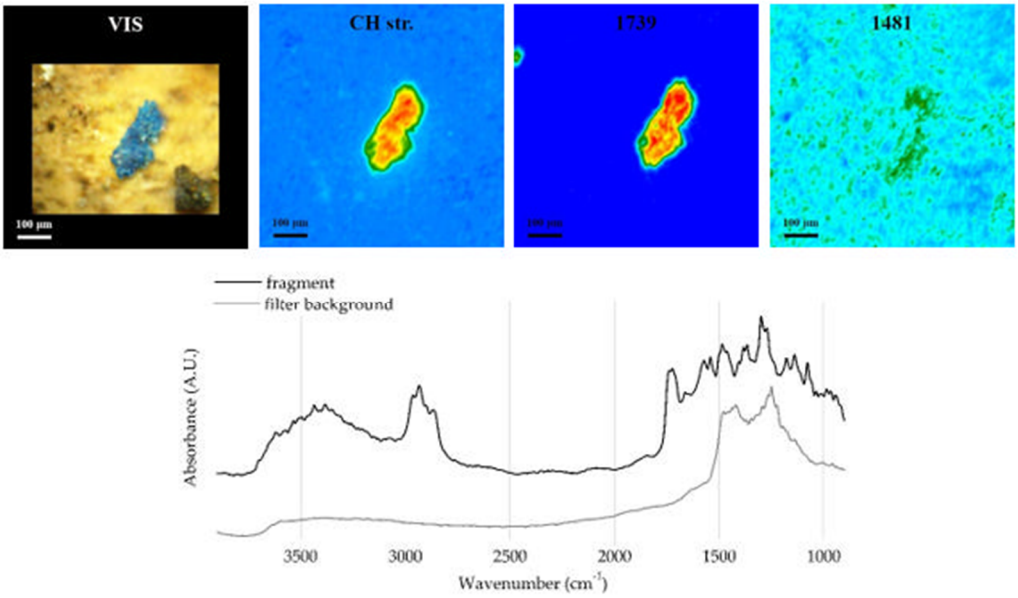

Figure S7. (From the left) Visible light and 2D FTIR Imaging maps of a fragment identified as ethylene-vinyl acetate (EVA) owing to absorption ~3300 cm^{-1} (OH stretching), 3000-2850 cm^{-1} (CH stretching), 1739 cm^{-1} (C=O stretching), 1481 cm^{-1} (CH_2 and CH_3 bending), 1389 cm^{-1} (CH_3 bending), 1281 cm^{-1} (C(=O)O stretching) [91]. (Bottom) FTIR Reflectance spectra of the polymer fragment and of the filter background, relating to a single pixel (5.5 × 5.5 μm^2) of the 2D Imaging map.

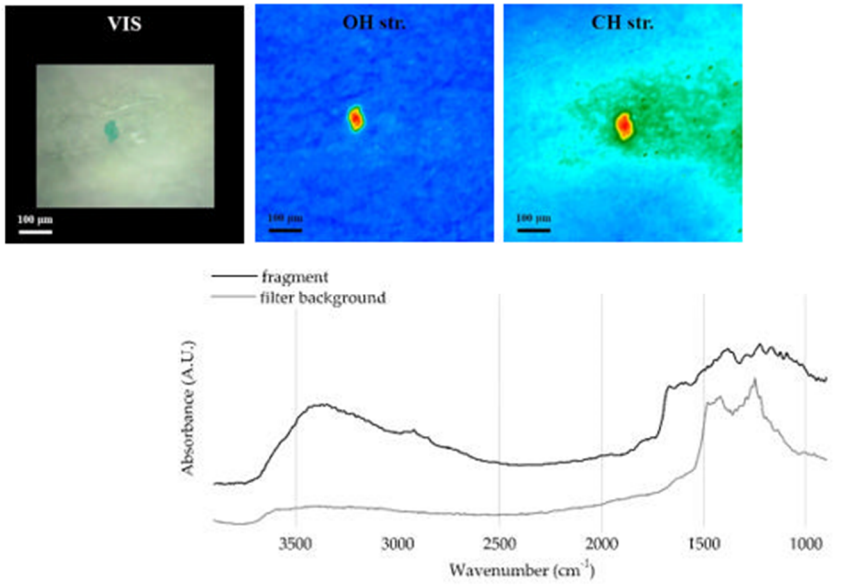

Figure S8. (From the left) Visible light and 2D FTIR Imaging maps of a fragment identified as polysaccharide gum owing to absorption ~3500 cm^{-1} (OH stretching), 3000-2800 cm^{-1} (C=O stretching), 1674 and 1580 cm^{-1} (C=C stretching), and 1382 cm^{-1} (CH bending) [93,94]. Although the similarity with the cellulose spectrum, the shape of the item and the presence of several functional groups allowed the above-mentioned polymeric assignment. (Bottom) FTIR Reflectance spectra of the polymer fragment and of the filter background, relating to a single pixel (5.5 × 5.5 μm^2) of the 2D Imaging map.

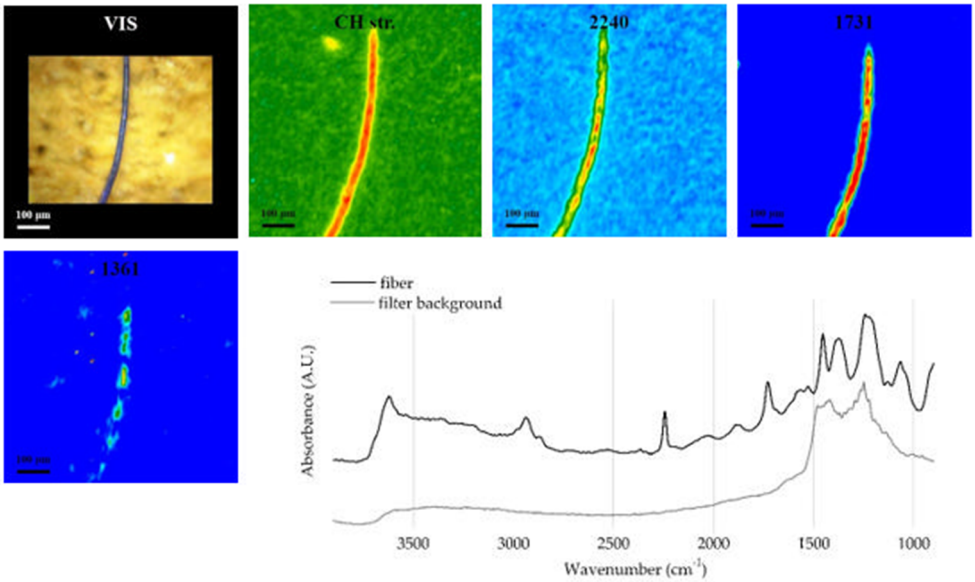

Figure S9. (From the left) Visible light and 2D FTIR Imaging maps of a fiber identified as polyacrylonitrile (PAN) owing to absorption 2930 and 2872 cm^{-1} (=C-H stretching), 2240 cm^{-1} (CN stretching), 1731 cm^{-1} (C=O stretching probably due to oxidation), 1455 and 1361 cm^{-1} (CH_2 bending), and 1068 cm^{-1} (CH stretching) [91,95]. (Bottom) FTIR Reflectance spectra of the polymer fiber and of the filter background, relating to a single pixel (5.5 × 5.5 μm^2) of the 2D Imaging map.

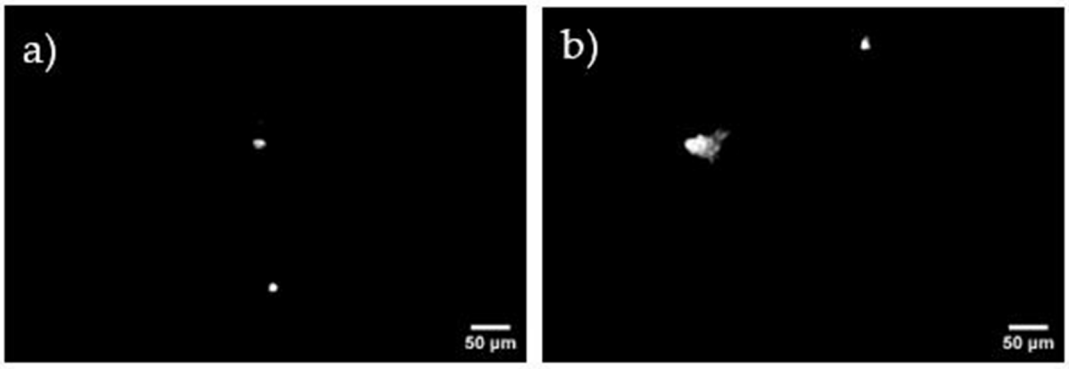

Figure S10. Example of a) polymer pellets from the Harpacticoida pool and b) polymer fragment and pellet from the Ostracoda pool visualized at the epifluorescence microscope (ex: 455-495 nm; em. 515-625 nm).

S11. Micro-computed tomography (µ-CT)

Micro-computed tomography (µ-CT) analysis was performed on *P. franciscoloi* adult female, approximately 5 mm in length. The samples were analyzed by collecting µ-CT data using Skyscan 1172 high-resolution microCT. This system has a sealed, microfocus tungsten X-ray tube with a 5 µm focal spot size. The X-ray was produced by exposing the anode to an electron beam at a range of 60 kV and 150 µA. Each sample was placed on a pedestal between the X-ray tube source and the charge-coupled device detector. The 2D X-ray images were captured with a slice-to-slice rotation angle range of 0.3°. The spatial resolution of the images was kept at 11 µm in terms of pixel size. The 3D image of the object's internal structure was reconstructed using a modified Feldkamp algorithm for cone-beam acquisition geometry, realized in Nrecon v.1.6.3.3 software. The alignment and beam hardening corrections were made before starting the re-construction process. CTVox program was used for 3D visualization, while CT-Analyser (CTan) software was used for the image clean up and measurements.

Reference

90. Garside, P.; Wyeth, P. Identification of Cellulosic Fibres by FTIR Spectroscopy: Thread and Single Fibre Analysis. Stud Conserv 2003, 48, 10.2307/1506916
91. Jung, M.R.; Horgen, F.D.; Orski, S.V.; Rodriguez C.V.; Beers, K.L.; Balazs, G.H.; Jones, T.T.; Work, T.M.; Brignac, K.C.; Royer, S.J.; Hyrenbach, K.D.; Jensen, B.A.; Lynch, J.M. Validation of ATR FT-IR to identify polymers of plastic marine debris, including those ingested by marine organisms. Mar Pollut Bull 2018, 127, 704–716. https://doi.org/10.1016/j.marpolbul.2017.12.061
92. Wang, C.; Wang, Y.; Dang, Y.; Jiao, Q.; Li, H.; Wu, Q.; Zhao, Y. Synthesis of a novel titanium complex catalyst and its catalytic performance for olefin polymerization. Russ J Appl Chem 2015, 88, 1723–1727. https://doi.org/10.1134/S1070427215100262
93. Faria, S.; De Oliveira Petkowicz, C.L.; De Morais, S.A.L.; Terrones, M.G.H.; De Resende, M.M.; De Frana, F.P.; Cardoso, V.L. Characterization of xanthan gum produced from sugar cane broth. Carbohydr Polym 2011, 86, 469–476. https://doi.org/10.1016/j.carbpol.2011.04.063
94. Hong, T. Nie, S.-P.; Xie, M.-Y. Applications of infrared spectroscopy in polysaccharide structural analysis: Progress, challenge and perspective. Food Chem 2012, 12, 100168. https://doi.org/10.1016/j.fochx.2021.100168
95. Mizher, R.M.; H. Adawiya, J.; Naser, J.Z.; Wee, T.T.; Zaki B, A.R.M.; Bin, K.A. Synthesis and characterization of grafted Ac-rylonitrile on Polystyrene modified with carbon nanotubes using Gamma-irradiation. Res J Chem Sci 2012, 2, 790-795. 10.5897/SRE11.1286